

Charging and emission effects of multiwalled carbon nanotubes probed by electric force microscopy

M. Zdrojek

Institut d'Electronique et de Microelectronique et de Nanotechnologie, CNRS UMR 8520, Avenue Poincaré, F-59652 Villeneuve d'Ascq, France and Faculty of Physics, Warsaw University of Technology, Koszykowa 75, 00-662 Warsaw, Poland

T. Mélin,^{a)} C. Boyaval, and D. Stiévenard

Institut d'Electronique et de Microelectronique et de Nanotechnologie, CNRS UMR 8520, Avenue Poincaré, F-59652 Villeneuve d'Ascq, France

B. Jouault

Groupe d'Etude des Semiconducteurs, CNRS UMR 5650, Université Montpellier II, Place Eugène Bataillon, 34095 Montpellier Cedex 05, France

M. Wozniak

Faculty of Materials Science and Engineering, Warsaw University of Technology, ul. Woloska 141, 02-507 Warsaw, Poland

A. Huczko

Faculty of Chemistry, University of Warsaw, ul. Pasteura 1, 02-093 Warsaw, Poland

W. Gebicki and L. Adamowicz

Faculty of Physics, Warsaw University of Technology, Koszykowa 75, 00-662 Warsaw, Poland

(Received 8 September 2004; accepted 24 March 2005; published online 20 May 2005)

Electrostatic properties of single-separated multiwalled carbon nanotubes (MWCNTs) deposited on a dielectric layer have been investigated by charge injection and electric force microscopy (EFM) experiments. We found that upon local injection from the biased EFM tip, charges delocalize over the whole nanotube length (i.e., 1–10 μm), consistent with a capacitive charging of the MWCNT-substrate capacitance. In addition, the insulating layer supporting the nanotubes is shown to act as a charge-sensitive plate for electrons emitted from the MWCNTs at low electric fields, thus allowing the spatial mapping of MWCNT field-emission patterns. © 2005 American Institute of Physics. [DOI: 10.1063/1.1925782]

The control of electrostatic properties of carbon nanotubes is of fundamental interest for potential applications such as field-emission electron sources. However, although field emission from single-separated multiwalled carbon nanotubes (MWCNTs), or arrays of MWCNTs (Refs. 1 and 2), were reported nearly one decade ago,³ the understanding of the MWCNT field-emission processes from their atomic structure is still in progress both from a theoretical⁴ and experimental point of view.⁵ In this letter, we investigate the electrostatic properties of single-separated MWCNTs by charge injection and electric force microscopy (EFM) experiments.⁶ We found that upon local injection from the biased EFM tip, excess charges delocalize over the whole nanotube length (i.e., 1–10 μm), consistent with a capacitive charging of the MWCNT-substrate capacitance. However, for nanotubes with smaller diameters, drastic changes are observed in their electrostatic properties, with the occurrence of abrupt discharging behaviors. In addition, the dielectric layer supporting the nanotubes is shown to act as an efficient trap for the electrons emitted from the MWCNTs, thus allowing the spatial mapping of MWCNT field emission patterns.

MWCNTs were grown by chemical vapor deposition using Ni particles as catalysts.⁷ After a nitric acid treatment to separate the metal particles from the grown MWCNTs, purified nanotubes in powder form were immersed in dichloromethane, ultrasonically agitated for a few hours, and then

dispersed by spin coating on substrates. Typical transmission electron microscopy micrographs of the MWCNTs are given in Figs. 1(a) and 1(b), showing the organization of the graphene sheets and typical MWCNT cap shapes. For electrical characterization purposes, nanotubes were dispersed onto a thin (200 nm) thermal oxide layer on a silicon wafer with resistivity 0.01 $\Omega\text{ cm}$ (later also used for the EFM experiments). Electrical contacts were achieved on single-separated MWCNTs using a dual ion- and electron-beam microscope (FEI Strata DB 235), and by directly writing Pt contacts on top of a given MWCNT (Ref. 8) [see Fig. 1(c)]. The ohmic behavior of contacted MWCNTs at 300 K was checked using two and four-probe measurements [see Fig. 1(d)].

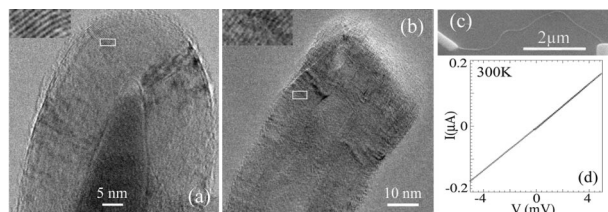


FIG. 1. (a) and (b) Typical transmission electron microscopy images of MWCNT caps. Insets: Magnified data associated with the white frames and showing the local graphene plane structure. (c) Scanning electron micrograph of a single-separated MWCNT on a 200 nm thick SiO₂ layer with platinum electrical contacts deposited by a focused ion-beam apparatus. (d) Room-temperature current-voltage characteristics of the MWCNT of Fig. 1(c) showing an ohmic behavior (31 k Ω resistance).

^{a)}Electronic mail: thierry.melin@isen.iemn.univ-lille1.fr

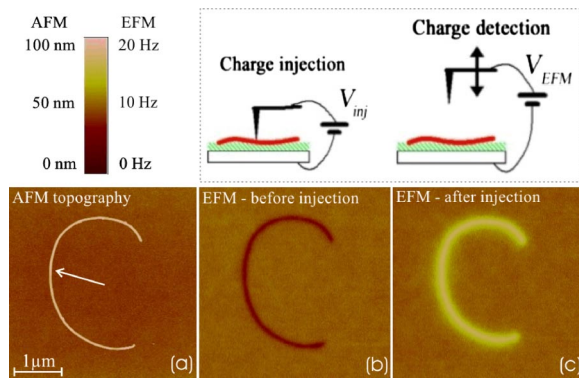


FIG. 2. Inset: (left) Schematics of the charge injection with the tip biased at V_{inj} with respect to the substrate; (right) EFM data acquisition, consisting in recording the EFM cantilever resonance frequency shifts, when biased at V_{EFM} . (a) Atomic force microscopy topography image of a MWCNT with ~ 30 nm diameter. The scale bar is $1 \mu\text{m}$. (b) EFM image ($V_{EFM} = -2$ V) of the uncharged nanotube (20 Hz color scale). (c) EFM image ($V_{EFM} = -2$ V) after charge injection ($V_{inj} = -3$ V for 2 min).

Charge injection and EFM experiments were performed at 300 K under dry nitrogen atmosphere with a Nanoscope IIIa microscope (Veeco). We used PtIr-coated cantilevers with frequency ~ 60 kHz and spring constant ~ 2 – 5 N/m. Charge injection is achieved by pressing the EFM tip biased at V_{inj} —with respect to the silicon substrate—with a typical 2 nN contact force on a given nanotube for a few minutes (see Fig. 2, inset). The resulting transfer of charges along the nanotubes is then characterized by EFM, in which electric force gradients acting on the tip biased at V_{EFM} shift the EFM cantilever frequency.⁶ In practice, the acquisition of EFM data is interleaved line by line during the sample topography imaging where the tip is grounded. Experiments are illustrated in Fig. 2 for a nanotube with ~ 30 nm diameter [see Fig. 2(a) for the topography image]. In EFM images, MWCNTs are always observed prior to injection as a dark feature (negative frequency shift) [Fig. 2(b), $V_{EFM} = -2$ V]. This signal accounts for the local increase of the tip-substrate capacitance when the EFM tip is moved over MWCNTs and is proportional to $-V_{EFM}^2$.⁶ After the charge injection (here using $V_{inj} = -3$ V for 2 min), the nanotube EFM image [Fig. 2(c), $V_{EFM} = -2$ V] exhibits a bright contrast corresponding to a positive frequency shift. This is due to the interaction between the MWCNT charge Q_{NT} and capacitive charges at the tip apex (which here dominates over capacitive effects). Since this charge frequency shift varies as $Q_{NT} \cdot V_{EFM}$, the positive feature observed in Fig. 2(c) demonstrates that $Q_{NT} < 0$, i.e., there is a storage of electrons along the nanotube. No discharge could be observed upon continuous scanning for 10 h for the MWCNT of Fig. 2.

The delocalization of excess charges over microns upon local injection from the EFM tip apex is a consequence of the conductive nature of the MWCNT and attributed to the charging of the MWCNT-substrate capacitor. This is supported by the 300 K metallic behavior of the MWCNTs at low bias [see Fig. 1(d)], enabling the delocalization of injected charges. Also, preliminary $Q_{NT}(V_{inj})$ spectroscopic measurements indicate an overall general linear behavior, which is consistent with a capacitive charging of the MWCNTs.⁹ Using a model derived from Ref. 6, we estimated from EFM experiments the linear density of the charged MWCNT: $|\lambda| \sim 20$ – 50 e/ μm . This value is then compared to the prediction of a pure capacitive model, tak-

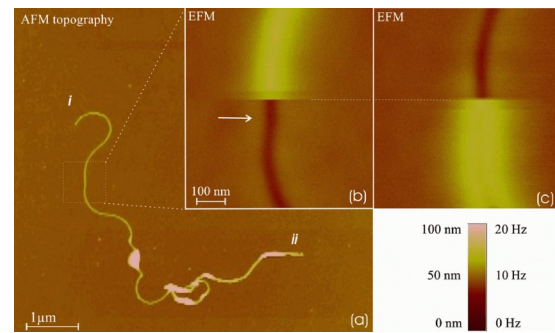


FIG. 3. (a) Atomic force microscopy image of a $\sim 15 \mu\text{m}$ long MWCNT. The local nanotube diameter is, respectively, 18 and 30 nm in the vicinity of its two caps labelled (i) and (ii). (b) and (c) EFM scans ($V_{EFM} = -2$ V, 20 Hz color scale, 20 min acquisition time) after charge injection experiments ($V_{inj} = -6$ V, 2 min). The injections in (b) and (c) were performed at the point indicated by the arrow. Scans were acquired from top to bottom in (b) and from bottom to top in (c), showing that the abrupt discharge is related to a specific point of the MWCNT. The dashed line is a guide for the eye for the correspondence between the two EFM images.

ing $C/L = 2\pi\epsilon_0/\ln(2d/r_0)$ for the linear capacitance of a cylindrical metal wire of radius r_0 separated in air by a distance d from a metal plane (with here $r_0 \ll d$). We obtain $|\lambda| \sim 300$ e/ μm for an injection bias $|V_{inj}| = 3$ V, $d = 200$ nm, and $r_0 = 15$ nm. The discrepancy between the estimation and experimental values is likely to originate in the very details of the MWCNT charging mechanisms. Such a description falls by far beyond the scope of this letter.

We now report on the change of electrostatic properties observed for smaller nanotubes. This is illustrated in Fig. 3, showing the topography image of a $\sim 15 \mu\text{m}$ long MWCNT [Fig. 3(a)], and exhibiting two different diameters around its two caps, i.e., 18 nm and 30 nm, respectively, for the upper and lower cap regions labelled (i) and (ii). A charge injection experiment ($V_{inj} = -6$ V, 2 min) was performed in the vicinity of cap (i) (local nanotube diameter ~ 18 nm). In Fig. 3(b), the EFM image after charge injection is scanned from top to bottom ($V_{EFM} = -2$ V, 20 min) scan duration). The bright feature associated with negative stored charge is seen to disappear at midscan within a few scan lines, leaving the nanotube uncharged on the surface, as seen from its corresponding dark EFM feature after discharge [Fig. 3(b), bottom]. To demonstrate that the abrupt discharge is associated with a specific point of the MWCNT, the charging experiment was repeated at the same injection point, and the EFM detection was performed in similar conditions apart from the scan direction set from bottom to top in Fig. 3(b). This also revealed an abrupt discharge at the same nanotube point. From the small amount of negative charges left on the oxide after the discharge [faint bright halo surrounding the nanotube in Fig. 3(b), bottom, or in Fig. 3(c), top], we conclude that the electrons initially stored in the MWCNT have been emitted from the nanotube to the grounded tip apex during the topography imaging. A possible explanation for the abrupt discharge points observed along the MWCNTs with smaller diameters would correspond to the presence of structural defects enhancing the field emission of electrons from the nanotube to the tip apex during the topography imaging. This is, first of all, supported by the disordered structure of graphene sheets along the nanotubes [see Figs. 1(a) and 1(b)]. Also, in all our measurements, abrupt discharges could be observed either along the MWCNTs, but also at the nanotube caps as well, and in any case only for local nanotube diameters smaller

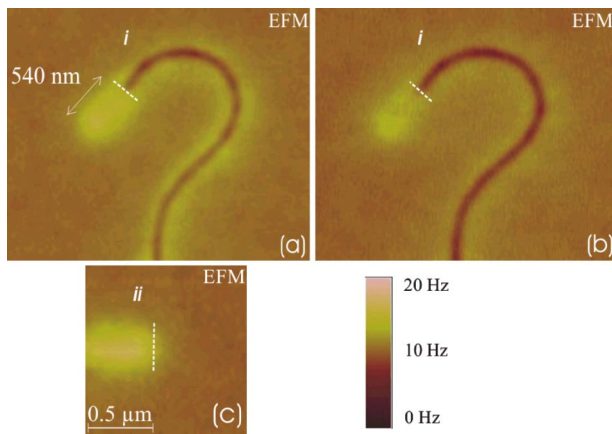


FIG. 4. (a) EFM image ($V_{\text{EFM}} = -2$ V) of the cap region (i) of the MWCNT of Fig. 3 acquired after the charging and discharging experiments of Fig. 3(b) and 3(c). The bright halo corresponds to negative charges on the oxide surface. The dotted line is a guide-to-the-eye for the MWCNT cap to emphasize the enhanced electron emission over ~ 500 nm. (b) Same scan taken 14 h later, showing a weak decay of oxide charges. (c) EFM image ($V_{\text{EFM}} = -2$ V) of the cap region (ii) after charging (no abrupt discharge could be observed in the vicinity of this cap), showing the MWCNT negative charges, but no enhanced emission at the cap.

that 25 nm. This shows that the emission is enhanced for smaller diameters, thus discarding any potential discharging mechanism mediated by external dirt on the nanotube side and caps, and supporting rather a field-emission mechanism for the discharge.

This is further confirmed by the electron emission properties observed at the MWCNT caps. We first discuss the cap (i) following the charging/discharging experiments reported in Fig. 3. In Fig. 4(a), the vicinity of the cap (i) is displayed after the charging/discharging experiments of Figs. 3(b) and 3(c). The nanotube appears as a dark feature in Figs. 4(a) and 4(b) demonstrating its neutral character after the experiments of Fig. 3. However, as seen from Fig. 4(b), it is surrounded by a slightly bright halo after the charging/discharging experiments, corresponding to negative charges emitted from the nanotube to the oxide surface. At the nanotube cap [the dashed line in Fig. 4(a) is a guide to the eye], the electron emission is found to be dramatically enhanced over ~ 500 nm along the nanotube axis, with an opening half angle less than 5° .¹⁰ The oxide layer appears as a practical charge-sensitive plate for the emission processes, since the emission pattern is typically unchanged after 14 h continuous scanning, as seen from Fig. 4(b). From the electron emission enhancement along the nanotube, and the high anisotropy of the observed emission patterns, we deduce that the local field created at the nanotube cap is the driving force for the emission process. However, one cannot strictly speaking distinguish between a mechanism where charges are directly field emitted onto the oxide surface, and a two-step mechanism, where charge emission occurs in the vicinity of the tip cap in combination with a migration of emitted charges on the oxide due to the electric field at the cap of the charged MWCNT. However, such a charge migration can obviously only be efficient provided the nanotube is still charged. This is demonstrated in Fig. 4(b), where the lateral resolution of the charge emission pattern is unchanged compared to Fig. 4(a) after 14 h of continuous scanning. More quantitatively, considering the tip injection voltage $V_{\text{inj}} = -6$ V and the 200 nm thickness of the SiO_2 layer, one can estimate a 0.03 V/nm average electric field between the nanotube and

the substrate. Emission at low field would, therefore, occur for a MWCNT with field enhancement factor of the order of ~ 100 , which is likely for a MWCNT with diameter ~ 18 nm.¹¹ However, such a few V/nm local electric field is sufficient to induce an enhanced charge migration in the SiO_2 layer along the nanotube, suggesting that field emission and electric-field induced transport in the oxide layer probably combine during the discharge to lead to the electron emission patterns observed in Figs. 4(a) and 4(b).

Finally, the same nanotube was scanned after charge injection [Fig. 4(c)] around its second cap (ii) with a diameter of 30 nm. No abrupt discharge was observed during scanning, either along the nanotube or directly at the cap. Consequently, the negatively charged nanotube cap leads to the bright EFM feature observed in Fig. 4(c). No enhanced electron emission could be observed beyond the nanotube cap, in contrast with Figs. 4(a) and 4(b). This underlines the correlation between the abrupt discharge behavior and the enhanced electron emission patterns on the oxide surface, together with the nanotube cap and diameter size.

In conclusion, we investigated the charging and emission effects of MWCNTs by EFM. The charge delocalization is consistent with an injection mechanism based on the charging of the MWCNT-substrate capacitance. We found that MWCNTs with smaller diameters exhibit abrupt discharging and enhanced electron emission properties. These results appear very promising to study experimentally the spatial field-emission properties of model systems, such as single or double-walled carbon nanotubes.

The authors thank H. Diesinger, D. Deresmes, G. Allan, and C. Delerue for fruitful discussions. We acknowledge IRCICA, the European Community's Human Potential Programme under Contract No. HPRN-CT-2002-00320, NANOSPECTRA, and the CEPHOMA centre of excellence for financial support.

¹A. G. Rinzler, J. H. Hafner, P. Nikolaev, L. Lou, S. G. Kim, D. Tomanek, P. Nordlander, D. T. Colbert, and R. E. Smalley, *Science* **269**, 1550 (1995).

²W. Heer, W. S. Bacsá, A. Châtelain, and D. Ugarte, *Science* **270**, 1179 (1995).

³For a recent review, see J. M. Bonard, M. Croci, C. Klinke, R. Kurt, O. Noury, and N. Weiss, *Carbon* **40**, 1715 (2002).

⁴X. Zheng, G. Chen, Z. Li, S. Deng, and N. Xu, *Phys. Rev. Lett.* **92**, 106803 (2004); A. Buldum and J. P. Lu, *ibid.* **91**, 236801 (2003); C. Adessi and M. Devel, *Phys. Rev. B* **65**, 075418 (2002); A. Mayer, N. M. Miskovsky, and P. H. Cutler, *ibid.* **65**, 155420 (2002).

⁵See, e.g., J. M. Bonard, C. Klinke, K. A. Dean, and B. F. Coll, *Phys. Rev. B* **67**, 115406 (2003); S. T. Purcell, P. Vincent, C. Journet, and V. Thien Binh, *Phys. Rev. Lett.* **88**, 105502 (2002).

⁶T. Mélin, H. Diesinger, D. Deresmes, and D. Stiévenard, *Phys. Rev. Lett.* **92**, 166101 (2004); T. Mélin, H. Diesinger, D. Deresmes, and D. Stiévenard, *Phys. Rev. B* **69**, 035321 (2004).

⁷See J. M. Bonard, M. Croci, C. Klinke, F. Conus, I. Arfaoui, T. Stöckli, and A. Chatelain, *Phys. Rev. B* **67**, 085412 (2003) and references therein.

⁸T. W. Ebbesen, H. J. Lezec, H. Hiura, J. W. Bennett, H. F. Ghaemi, and T. Thio, *Nature (London)* **382**, 54 (1996).

⁹However, pronounced hysteresis appear in $Q_{\text{NT}}(V_{\text{inj}})$ curves when the injection bias V_{inj} is cycled. Such effects have already been observed in the case of in silicon nanoparticles, where the charge memory effect was associated with surface charges: H. Diesinger, T. Mélin, D. Deresmes, D. Stiévenard, and T. Baron, *Appl. Phys. Lett.* **85**, 3546 (2004).

¹⁰Y. Saito, K. Hamaguchi, K. Hata, K. Uchida, Y. Tasaka, F. Ikazaki, M. Yumura, A. Kasuya, and Y. Nishina, *Nature (London)* **389**, 554 (1997); N. de Jonge, Y. Lamy, K. Schoots, and T. H. Oosterkamp, *ibid.* **420**, 393 (2002).

¹¹L. Nilsson, O. Groening, C. Emmenegger, O. Kuettel, E. Schaller, L. Schlappbach, H. Kind, J. M. Bonard, and K. Kern, *Appl. Phys. Lett.* **76**, 2071 (2000).